Materials Letters 276 (2020) 128183

Contents lists available at ScienceDirect

Materials Letters

journal homepage: www.elsevier.com/locate/mlblue

On the difference in carbon- and nitrogen-alloying of equiatomic FeMnCrNiCo high-entropy alloy

E.G. Astafurova *, K.A. Reunova, E.V. Melnikov, M.Yu. Panchenko, S.V. Astafurov, G.G. Maier, V.A. Moskvina

Institute of Strength Physics and Materials Science SB RAS, 2/4 Akademicheskii ave., 634055 Tomsk, Russia

ARTICLE INFO

Article history:
Received 4 June 2020
Received in revised form 18 June 2020
Accepted 18 June 2020
Available online 20 June 2020

Keywords:
High-entropy alloy
Solid-solution strengthening
Austenite
Carbon
Nitrogen

ABSTRACT

Microstructure and tensile properties of $Fe_{20}Mn_{20}Cr_{20}Ni_{20}Co_{20}$, $Fe_{20}Mn_{20}Cr_{20}Ni_{20}Co_{20-x}C_x$ and $Fe_{20}Mn_{20}Cr_{20}Ni_{20}Co_{20-x}N_x$ (x = 1 at.% and 3 at.%) high-entropy cast alloys have been studied. Interstitial-doped alloys possess an austenitic structure with expanded crystal lattice and dendritic segregations of the alloying elements. Alloying with 1 at.% of C or N provides high solid-solution strengthening effects. Despite inhomogeneous dendritic microstructure, a yield strength and an elongation (349 MPa and 59%) in $Fe_{20}Mn_{20}Cr_{20}Ni_{20}Co_{17}N_3$ alloy exceed those for N-free alloy (163 MPa and 55%). Carbon-alloying produces more inhomogeneous microstructure and a precipitate hardening as compared to nitrogen-alloying and is accompanied with embrittlement of $Fe_{20}Mn_{20}Cr_{20}Ni_{20}Co_{17}C_3$ alloy.

1. Introduction

In 2004, Cantor and Yeh have been published the first results concerning the design of multicomponent high-entropy alloys [1,2]. Initially, alloys of this class have contained five or more elements in near-equiatomic concentrations but further a family of high-entropy alloys has been completed by a variety of multicomponent non-equiatomic systems [3–5]. In last decade the heterophase alloys attract attention from materials scientists [3–6]. The comprehensively studied composition, the equiatomic FeCrMnNiCo Cantor alloy [1], possesses FCC crystal structure and demonstrates an excellent ductility at room and cryogenic temperatures but a relatively low yield strength [1,7,8]. Interstitial-alloying is a promising way to improve strength properties of high-entropy alloys via both solid-solution hardening and precipitation strengthening, but interstitially-doped alloys could suffer from the negative influence of precipitates on ductility [9–18].

Some researcher [14,18,19] have reported that carbon-alloying could simultaneously increase strength of high-entropy alloys at the maintenance of high plasticity. But the general trend is that increase in carbon content promotes the complex hardening mechanism in FeCrMnNiCo-type alloys: solid-solution strengthening, precipitate hardening and carbide-assisted grain refinement [13,17,18]. Very limited data exist about the N-alloyed of FeMnCrNiCo-type alloys. Y. Xie et al. [12] and I. Moravcik et al. [10] have obtained N-doped FeMnCrNiCo alloys using mechanical alloying with following vacuum hot pressing sintering and by reactive powder milling. These methods do not allow to obtain pure austenitic phase in high-entropy alloy because numerous precipitates complicate the analysis [10,12]. Cast CoCrNiN alloy (0.5 at.% N) possesses a stable microstructure without nitrides, and nitrogen-alloying causes 24–33% increase in the yield strength at identical ductility with N-free alloy [9].

In this study we evaluate and compare the effects of nitrogen and carbon with concentrations up to 3 at. % on the microstructure, phase composition and mechanical properties on FeMnCrNiCo high-entropy alloy.

2. Materials and methods

Five ingots with chemical compositions $Fe_{20}Mn_{20}Cr_{20}Ni_{20}Co_{20}$ (HEA, at. %), $Fe_{20}Mn_{20}Cr_{20}Ni_{20}Co_{19}C_1$ (HEA-1C), $Fe_{20}Mn_{20}Cr_{20}Ni_{20}Co_{17}C_3$ (HEA-3C), $Fe_{20}Mn_{20}Cr_{20}Ni_{20}Co_{19}N_1$ (HEA-1N) and $Fe_{20}Mn_{20}Cr_{20}Ni_{20}Co_{17}N_3$ (HEA-3N) were produced by vacuum induction melting and casting in pure Ar atmosphere. Rectangular dumbbell shaped flat tensile specimens of 12 × 2.6 × 1.4 mm in gauge section were cut from the cast (as-solidified) material by electrical discharge machining. Tensile specimens were mechanically grinded and electrolytically polished. The specimens were tensile tested at room temperature and a strain rate of 5×10^{-4} s^{-1} using

* Corresponding author.
E-mail address: elena.g.astafurova@gmail.com (E.G. Astafurova).

https://doi.org/10.1016/j.matlet.2020.128183
0167-577X/

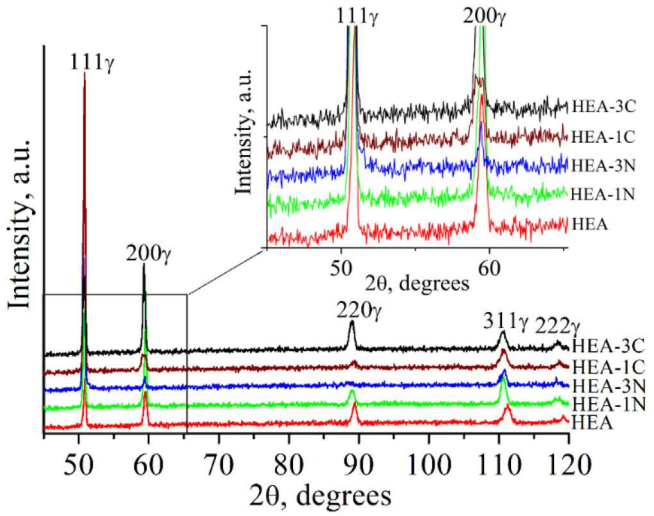

Fig. 1. XRD patterns for the cast HEAs with different interstitial contents.

electromechanical machine LFM-125 (Walter and Bai). The X-ray diffraction (XRD) analysis was done using DRON 7 diffractometer with Co-K_α radiation. Analysis of the microstructure was performed with a Philips SEM-515 scanning electron microscope (SEM) equipped with energy dispersive X-ray analysis (EDS) unit.

3. Results and discussion

According to XRD data, cast alloys possess an austenitic structure, no carbide or nitride phases have been identified (Fig. 1). Both nitrogen and carbon cause an expansion of a crystal lattice and increase in a lattice parameter of austenite (Table 1). These results argue the formation of a solid solution of nitrogen and carbon in austenite. At close atomic concentrations, carbon provides lower lattice distortions than nitrogen (Table 1) which is in agreement with [9].

All alloys are characterized by inhomogeneous dendritic microstructure (Fig. 2) typical for as-solidified HEA [1,14,20]. Relative to equiatomic composition, dendrites are enriched with Fe, Cr and Co atoms but interdendritic areas – by Mn and Ni. Morphology of dendritic segregations does not principally vary with the alloying of the HEA with nitrogen but for HEA-3N alloy the fraction of interdendritic areas is visibly smaller than those for HEA and HEA-1N and they are clearly more rounded (Fig. 2a, b, c). Therefore, nitrogen, as alloying element, decreases the tendency to dendritic segregation in this alloy. The tendency to grain boundary decorating in HEA-3N alloy could evidence the small portion of grain boundary nitrides (Fig. 2c). SEM EDS analysis does not allow to resolve any grain-boundary precipitates in HEA-3N alloy.

For C-alloyed alloys, dendritic segregations are more pronounced and single thin layers of carbide phase along grain boundaries are rarely seen at lower carbon content (1 at. %) (Fig. 2d). Despite the different morphology of dendritic microstructure in C- and N-alloyed HEAs, interdendritic and dendritic areas in them have similar elemental compositions (Fig. 2). In HEA-3C alloy, the areas with a pearlite morphology are observed next to the grain boundaries (Fig. 2e). These colonies consist of plates or spherical areas with different compositions corresponded either to dendritic areas or enriched with Cr and C atoms. The latter are carbides typical for C-doped FeMnCrNiCo-type alloys and reported earlier in [14,15,17,18].

Solid-solution hardening of Cantor alloy by of nitrogen is accompanied with substantial increase in a yield strength (YS) and an ultimate tensile strength (UTS) (Fig. 3, Table 1). The elongations to fracture in nitrogen-bearing alloys are even higher than that for interstitial-free alloy. True stress vs. true strain diagrams for HEA-1N and HEA-3N alloys show similar ascending $\sigma(\varepsilon)$-dependence but strain-hardening rate obviously increases with increase in nitrogen content. The increment in YS due to increase in C_N is high but cannot be approximated by the linear dependence $YS(C_N)$. This confirms the data of SEM analysis about the inhomogeneity in distribution of nitrogen in HEA-3N alloy. For HEA-1N alloy, no evidences of nitride formation have been found and the value of the strength increment $YS_{HEA\text{-}1N}$-YS_{HEA} = 139 MPa is high and a bit lower than the value estimated using the data of I. Moravcik [9] for coarse-grained CoCrNi alloy (≈200 MPa/at. %). Despite even higher nominal atomic concentration of carbon in HEA-1C alloy than nitrogen in HEA-1N alloy, carbon shows lower strengthening effect in comparison with nitrogen (Table 1). The value of C-assisted increment in the YS for HEA-1C alloy $YS_{HEA\text{-}1C}$-YS_{HEA} = 119 MPa. This value agrees with data of Moravcik et al. [11] (113 MPa/at.% C in CoCrNi with 0.5 at. % C), Wu et al. [16] (120 MPa/at.% C in FeMnCoCrNi with 0.5 at.% C) and exceeds results reported by Klimova et al. [14] (67 MPa/at.% C in $CoCr_{0.25}FeMnNi$) and Chen et al. [15] (65 MPa/at.% C in $FeMnCoCrNiC_{0.1}$).

Similar to nitrogen-alloying, carbon-bearing HEA-1C alloy possesses higher strength properties relative to the interstitial-free HEA (Fig. 3, Table 1). Nevertheless, the elongation of HEA-1C specimen is visibly lower than those for HEA-1N and HEA alloys. This effect could be associated with the complete "wetting" phenomenon in portion of grain boundaries by carbide phase in HEA-1C alloy (Fig. 2d, insert), which has been previously confirmed to be responsible for the embrittlement in Fe-C alloys [21]. With increase in carbon content in HEA up to 3 at. %, further increase in strength properties occurs but plasticity drops, and stress–strain diagrams attain parabolic shape typical for plastic deformation of alloys containing coarse incoherent particles [13,18,22]. Such behavior is attributed to the inhomogeneous distribution of the alloying elements in as-solidified alloy and, primarily, to the tendency to form intragranular and grain-boundary carbides in HEA-3C alloy (Fig. 2e).

Table 1
Tensile properties and the lattice parameter of austenitic phase (a) in cast alloys. YS – the yield strength, UTS – the ultimate tensile stress, δ – elongation. The nominal concentrations of carbon and nitrogen in alloys are specified in column "Notations".

Notation	YS, MPa	UTS, MPa	δ, %	a, nm
HEA	163	684	55	0.3593
HEA-1N (0.21 mass.% / 0.84 at.% N)	302	1002	58	0.3608
HEA-3N (0.8 mass.% / 3.13 at.% N)	349	1115	59	0.3609
HEA-1C (0.23 mass.% / 1.07 at.% C)	282	920	48	0.3603
HEA-3C (0.6 mass.% / 2.82 at.% C)	306	646	13	0.3608

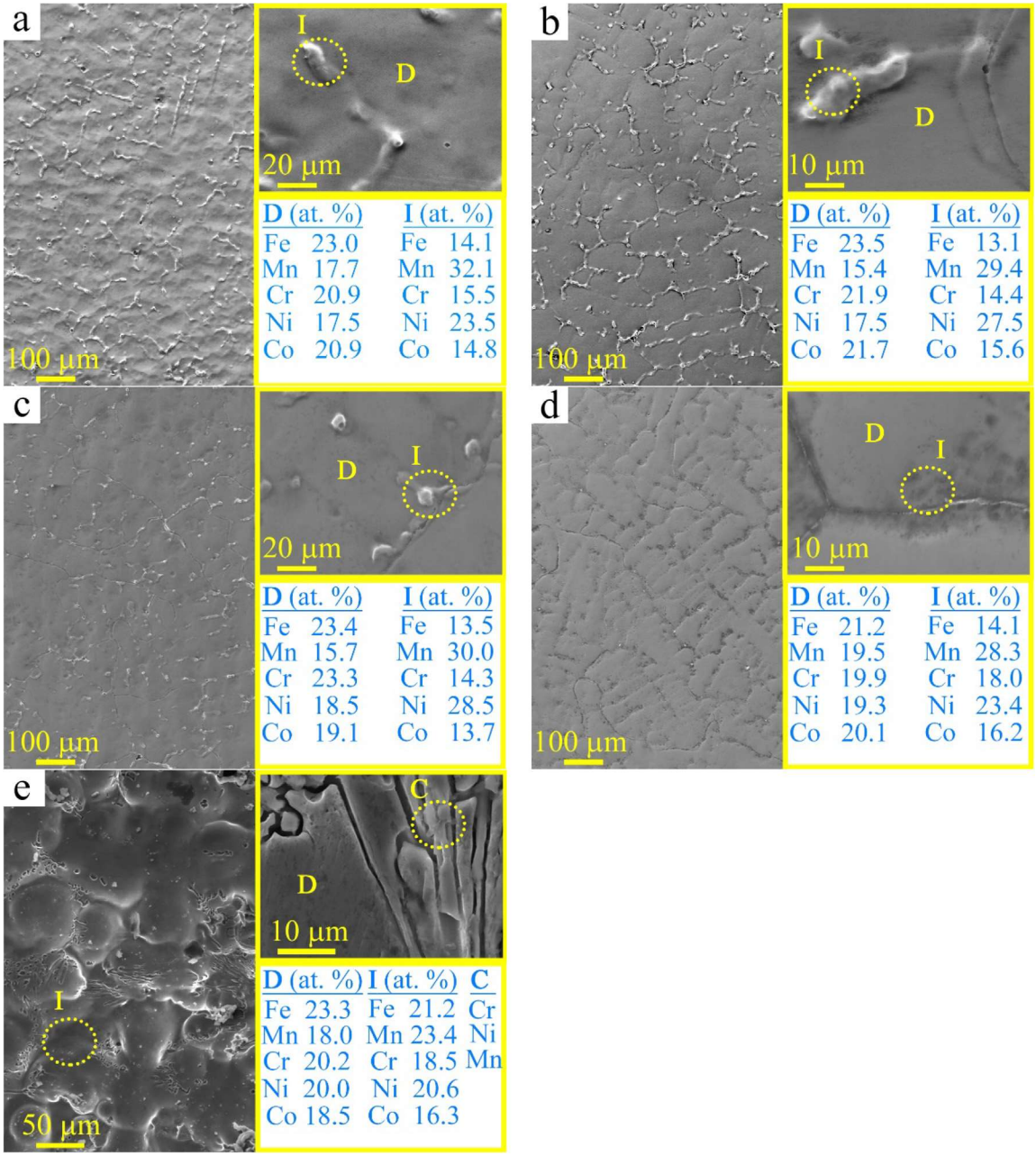

Fig. 2. Typical SEM images of the HEAs combined with EDS analysis: a – HEA, b – HEA-1N, c – HEA-3N, d – HEA-1C, e – HEA-3C. D – dendrite, I – interdendritic areas, C – carbide. For carbides in the image (e), an accurate elemental analysis is not presented because EDS analysis gives overestimated values for light elements like carbon and the observation area in SEM EDS analysis is higher than the thickness of the carbide plates.

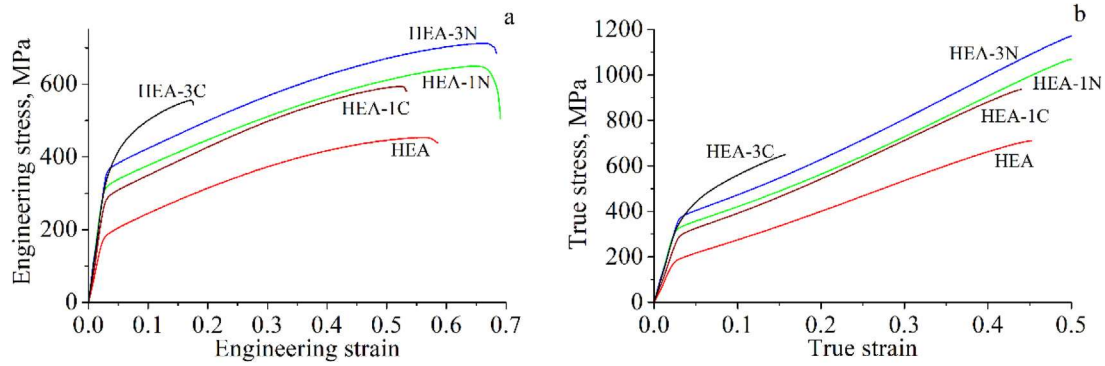

Fig. 3. Tensile engineering (a) and true (b) diagrams for cast alloys.

4. Conclusions

According to X-ray phase analysis, cast $Fe_{20}Mn_{20}Cr_{20}Ni_{20}Co_{20-x}C_x$ and $Fe_{20}Mn_{20}Cr_{20}Ni_{20}Co_{20-x}N_x$ (x = 1 at.% and 3 at.%) alloys possess austenitic structure independently on solute element (carbon or nitrogen) or interstitial concentration. Both nitrogen and carbon cause solid-solution strengthening which is accompanied with increase in strength properties of the alloys. Solid-solution hardening of the alloy by 1 at.% of C or N provides a substantial growth in strength properties at the preservation of high value of elongation to failure (about 160 MPa per at.% N and 110 MPa per at.% C). Carbon-doping provides weaker hardening and crystal lattice expansion of the high entropy alloy as compared to nitrogen. Despite inhomogeneity in distribution of the alloying elements in $Fe_{20}Mn_{20}Cr_{20}Ni_{20}Co_{17}N_3$ cast alloy and tendency to form grain-boundary precipitates, its yield strength and elongation (349 MPa and 59%) are higher than those for $Fe_{20}Mn_{20}Cr_{20}Ni_{20}Co_{20}$ alloy (163 MPa and 55%). Carbon-alloying up to 3 at.% produces more inhomogeneous microstructure in cast alloy and favors to precipitate hardening as compared to nitrogen-alloying which is accompanied with the embrittlement of $Fe_{20}Mn_{20}Cr_{20}Ni_{20}Co_{17}C_3$ alloy.

CRediT authorship contribution statement

E.G. Astafurova: Supervision, Conceptualization, Funding acquisition, Writing - original draft, Writing - review & editing. **K.A. Reunova:** Methodology, Investigation, Writing - original draft, Visualization. **E.V. Melnikov:** Methodology, Investigation, Data curation, Visualization. **M.Yu. Panchenko:** Investigation, Data curation, Formal analysis. **S.V. Astafurov:** Resources, Investigation, Project administration. **G.G. Maier:** Investigation, Data curation. **V. A. Moskvina:** Investigation, Data curation, Formal analysis.

Declaration of Competing Interest

The authors declare that they have no known competing financial interests or personal relationships that could have appeared to influence the work reported in this paper.

Acknowledgment

The research was supported by the Russian Science Foundation (project No. 20-19-00261).

References

[1] B. Cantor, I.T.H. Chang, P. Knight, A.J.B. Vincent, Mater. Sci. Eng. A 375–377 (2004) 213–218.
[2] J.W. Yeh, S.K. Chen, S.J. Lin, J.Y. Gan, T.S. Chin, T.T. Shun, C.H. Tsau, S.Y. Chang, Adv. Eng. Mater. 6 (2004) 299–303.
[3] Y. Zhang, T.T. Zuo, Z. Tang, M.C. Cao, K.A. Dahmen, P.K. Liaw, Z.P. Lu, Prog. Mater. Sci. 61 (2014) 1–93.
[4] D.B. Miracle, O.N. Senkov, Acta Mater. 122 (2017) 448–511.
[5] B.S. Murty, J.W. Yeh, S. Ranganathan, P.P. Bhattacharjee, Elsevier (2019) 388p.
[6] S. Gorsse, M.H. Nguyen, O.N. Senkov, D.B. Miracle, Data Brief 21 (2018) 2664–2678.
[7] F. Otto, A. Dloughy, Ch. Somsen, H. Bei, G. Eggeler, E.P. George, Acta Mater. 61 (2013) 5743–5755.
[8] A. Gali, E.P. George, Intermetallics 39 (2013) 74–78.
[9] I. Moravcik, H. Hadraba, L. Li, I. Dlouhy, D. Raabe, Z. Li, Scr. Mater. 178 (2020) 391–397.
[10] I. Moravcik, J. Cizek, L. de Almeida Gouvea, J. Cupera, I. Guban, I. Dlouhy, Entropy 21 (2018) 363.
[11] I. Moravcik, V. Hornik, P. Minarik, L. Li, I. Dlouhy, Mi Janovska, D. Raabe, Z. Li, Mater. Sci. Eng. A 781 (2020) 139242.
[12] Y. Xie, H. Cheng, Q. Tang, W. Chen, W. Chen, P. Dai, Intermetallics 93 (2018) 228–234.
[13] J.Y. Ko, S.I. Hong, J. Alloys Compd. (2018) 115–125.
[14] M.V. Klimova, A.O. Semenyuk, D.G. Shaysultanov, G.A. Salishev, S.V. Zherebtsov, J. Alloys Compd. 811 (152000) (2019) 1–10.
[15] J. Chen, Z. Yao, X. Wang, Y. Lu, X. Wang, Y. Liu, X. Fan, Mater. Chem. Phys. 210 (2018) 136–145.
[16] M. Wu, Z. Li, Mater. Sci. Eng. A 748 (2019) 59–73.
[17] L. Guo, X. Ou, S. Ni, Y. Liu, M. Song, Mater. Sci. Eng. A 746 (2019) 356–362.
[18] L.B. Chen, R. Wei, K. Tang, J. Zhang, F. Jiang, L. He, J. Sun, Mater. Sci. Eng. A 716 (2018) 150–156.
[19] Z. Wu, C.M. Parish, H. Bei, J. Alloys Compd. 647 (2015) 815–822.
[20] G.A. Salishchev, M.A. Tikhonovsky, D.S. Shaysultanov, N.D. Stepanov, A.V. Kuznetsov, I.V. Kolodiy, A.S. Tortika, O.N. Senkov, J. Alloys Compd. 591 (2014) 11–21.
[21] B.B. Straumal, Y.O. Kucheev, L.I. Efron, A.L. Petelin, J. Dutta Majumdar, I. Manna, J. Mater. Eng. Perf. 21 (2012) 667–670.
[22] D. Shaysultanov, N. Stepanov, S. Malopheyev, I. Vysotskiy, V. Sanin, S. Mironov, R. Kaibyshev, G. Salishchev, S. Zherebtsov, Mater. Char. 145 (2018) 353–361.